This document is downloaded from DR-NTU (https://dr.ntu.edu.sg)
Nanyang Technological University, Singapore.

Phase Evolution of M2 High Speed Steel During Selective Laser Melting: Experimental Investigation and Modelling

Liu, Zhong Hong; Zhang, Dan Qing; Chua, Chee Kai; Leong, Kah Fai

2014

Liu, Z. H., Zhang, D. Q., Chua, C. K., & Leong, K. F. (2014). Phase Evolution of M2 High Speed Steel During Selective Laser Melting: Experimental Investigation and Modelling. Proceedings of the 1st International Conference on Progress in Additive Manufacturing (Pro-AM 2014), 151-157.

https://hdl.handle.net/10356/84410

https://doi.org/10.3850/978-981-09-0446-3_099

© 2014 by Research Publishing Services.

Downloaded on 02 Dec 2022 05:01:10 SGT

PHASE EVOLUTION OF M2 HIGH SPEED STEEL DURING SELECTIVE LASER MELTING: EXPERIMENTAL INVESTIGATION AND MODELLING

Z. H. LIU
School of Mechanical and Aerospace Engineering, NTU Additive Manufacturing Centre, HW1-01-05, 2A Nanyang Link
Singapore, 637371, Singapore

D. Q. ZHANG, C. K. CHUA, K. F. LEONG
School of Mechanical and Aerospace Engineering, NTU Additive Manufacturing Centre, HW1-01-05, 2A Nanyang Link
Singapore, 637371, Singapore

ABSTRACT: This work studies the phase evolution in SLM where the resultant melt is considered as a moving volumetric heat source modeled as a double ellipsoidal heat source. The cooling rates and temperatures at different locations along the substrate and away from the heat source during the SLM process were simulated with the MATLAB program. Thermal gradient graphs were generated and the range of HAZ was identified from the corresponding theoretical austenitising temperature of M2 HSS. The associated HAZs were examined from their melt cross sections and validated with the simulated results. The evaluated HAZs from the experiments were found to be very close to the simulated HAZ range. The development of this model also provides the temperature distribution and cooling profiles in SLM.

INTRODUCTION

Background

Selective Laser Melting (SLM) is an Additive Manufacturing (AM) technique that produces physical 3-Dimensional (3D) parts in a layer by layer manner. Powder material is first deposited on a build platform and a powerful laser scans, melts and fuses the powder particles (Averyanova et al. 2011) to form an initial thin physical cross section of the model bonded to the platform (Liu et al. 2013). Subsequently, fresh layers of powder material are deposited and processed in a similar fashion (Chua et al. 2010). During the SLM process, the laser melts the powder material and re-melts the substrate material to a certain depth (Loh et al. 2014), thereby forming a melt consisting of both molten powder and substrate material. This melt fuses and bonds successive layers together upon solidification, forming a 3D part eventually. Generally, the bonding between successive layers is dependent on the size of melt and also the depth of melt penetration (Zhang et al. 2013).

Essentially, the substrate material surrounding the melt in the SLM process is heated to a temperature high enough (yet lower than the melting point of the material) to cause a phase transformation. The affected surrounding region is commonly known as the Heat Affected Zone (HAZ) and this occurs in several other laser related processes such as welding as discussed by Kou (2003) and surface melting as shown by Grum and Slabe (2006). As such, the HAZ in the SLM process can be modelled similarly to that of welding. In welding, the size of HAZ is dependent on several factors, primarily the laser power, laser scan speed and inherent alloy characteristics such as phase transformation temperatures. Lancaster (1999) suggested that in general, higher laser

Proc. of the Intl. Conf. on Progress in Additive Manufacturing
Edited by Chua Chee Kai, Yeong Wai Yee, Tan Ming Jen and Liu Erjia
Copyright © 2014 by Research Publishing Services.
ISBN: 978-981-09-0446-3 :: doi:10.3850/978-981-09-0446-3_099

power, slower scan speed and lower thermal diffusivity lead to a larger HAZ. HAZs are undesirable as they exhibit mechanical properties which are usually inferior to those of the base material. In Goldak's & Akhlaghi's (2005) research, it was mentioned that many failures of welds initiate in the coarse grained HAZ and hence much focus was put into controlling microstructure of HAZ by the welding engineers. Similarly in the SLM process, the developed HAZs within the microstructure may affect the properties of the produced part. Hence, it is important to model and characterise the HAZs in SLM parts in an attempt to control the degree of HAZ development and study the phase evolution during the process. For this purpose, M2 High Speed Steel (HSS) is used as a representative material for this study (Liu et al. 2011). A double ellipsoidal density heat source concept used in welding is proposed for the SLM process. This concept is used to model the moving volumetric heat source (which in this case is the melt) via programming with the MATLAB software. Simulations will be carried out in different laser scan speeds and substrate temperature conditions to generate thermal gradients and predict cooling rates which will in turn be validated experimentally.

MODELLING

Double ellipsoidal density heat source

The SLM machine used for this work is equipped with a 100 W Neodymium-doped Yttrium Aluminium Garnet (Nd:YAG) continuous wave (cw) laser with a wavelength of 1.064 nm and focus diameter 180 µm. The heat density is distributed in the Gaussian-distributed manner throughout the volume of the heat source from the laser, creating a spherical melt as shown in Figure 1a, where the bottom part of the melt beneath the substrate surface was approximated to be an ellipsoidal shape based on the observed form and considered to be a double ellipsoidal density heat source in a finite body. The double ellipsoidal was chosen over the single ellipsoidal density heat source because the simulation experience with a single ellipsoidal heat source model revealed that the temperature gradient in front of the heat source was not as steep as expected and the gentler gradient at the trailing edge of the melt was steeper. The double ellipsoidal heat source overcomes this limitation of the single ellipsoidal heat source whereby the front half (leading front) of the source is the quadrant of one ellipsoidal source and the rear half (trailing rear) is the quadrant of another ellipsoidal source as explained by Nguyen (2004). The double ellipsoidal heat source describing a resultant moving volumetric heat source with an ellipsoidal shape is shown in Figure 1b. This models closer to the actual moving volumetric heat source in the SLM process.

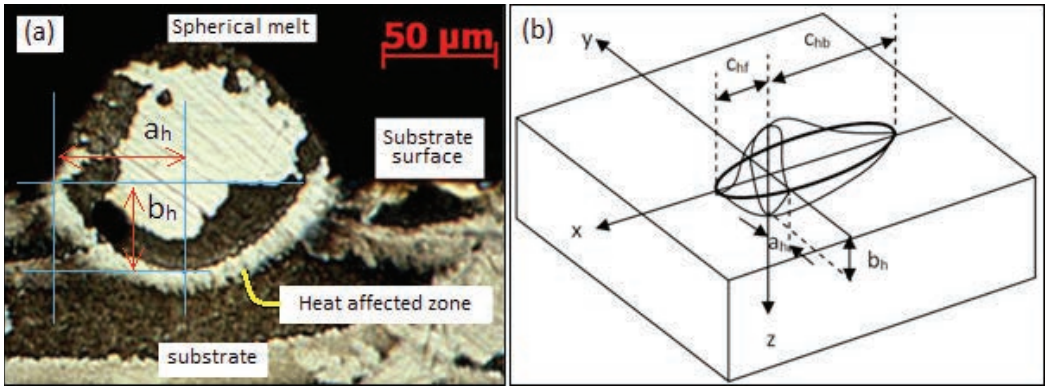

Figure 1. (a) Cross section of a melt in SLM and (b) double ellipsoidal density heat source.

The parameters a_h, b_h, c_{hf} and c_{hb} (where the subscripts *h* denotes half and *hf* and *hb* denote half front and half back respectively) are in fact the density heat source dimensions equivalent to those of the melt. This suggested that appropriate values for a_h, b_h, c_{hf} and c_{hb} could be obtained from the measurement of the melt geometry. Hence melt dimensions were measured and approximated as inputs for the parameters a_h, b_h, c_{hf} and c_{hb} proposed in this work. This is illustrated in Figure 1a. The measured radius, *r*, and depth, *d*, from the melt pool's cross section were directly taken as the values for a_h and b_h respectively. As for c_{hf} and c_{hb}, Nguyen (2004) explained that it was reasonable to assume that $c_{hf} = a_h$ and $c_{hb} = 2c_{hf}$ so as to simplify the situation based on the results found in most cases of practical applications.

Approximate analytical solution for a finite body

The substrate plate of length 0.1 m, width 0.1 m and thickness 0.02 m used in the SLM process is taken as the finite body denoted by length 2*L*, width 2*B* and thickness *D*, subjected to the double ellipsoidal heat source. The transient temperature for an arbitrary point (*x*, *y*, *z*) is therefore expressed as Eq. (1) (Nguyen 2004), where *Q*=effective power, ρ=density of substrate, *c*=specific capacity of substrate, *a*=thermal diffusivity of substrate, *t*=time limit for integration, *v*=laser scan speed, T_0=initial temperature of substrate at t=0s, *(x, y, z)*=location at time *t*, away from the initial location when t=0*s* and *T*=resultant temperature at *(x, y, z)*.

$$T - T_0 = \frac{3\sqrt{3}Q}{2\rho c\pi\sqrt{\pi}} \int_0^t \frac{\exp\left(-\frac{3y^2}{12a(t-t')+{a_h}^2} - \frac{3z^2}{12a(t-t')+{b_h}^2}\right) E(B,y,a_h).E(D,z,b_h)}{\sqrt{12a(t-t')+{a_h}^2}\sqrt{12a(t-t')+{b_h}^2}} \text{ x}$$

$$\left[\frac{r_f E(L,x-vt',c_{hf})\exp\left(-\frac{3(x-vt')^2}{12a(t-t')+{c_{hf}}^2}\right)}{\sqrt{12a(t-t')+{c_{hf}}^2}} + \frac{r_b E(L,x-vt',c_{hb})\exp\left(-\frac{3(x-vt')^2}{12a(t-t')+{c_{hb}}^2}\right)}{\sqrt{12a(t-t')+{c_{hb}}^2}}\right] dt' \quad (1)$$

According to basic heat transfer (neglecting radiation loss due to short laser and material interaction time) with the substrate having an initial temperature of T_0, effective laser power *Q* to create the melt can be calculated by Eq. (2) with the M2 HSS powder as the sample material and including the dense substrate as the heat sink as explained by Shao et al. (2001), where *m*= Mass of the melt under the process conditions, *T*=*s*olidus temperature of M2 HSS, *h*= Convective coefficient of M2 HSS, A_1= Cross section area of the ellipsoidal melt in the x-y plane as seen in Figure 2, A_2= Surface area of the ellipsoidal melt in contact with the substrate, λ= Heat conductivity coefficient of the surrounding medium and δ=Thickness of surrounding medium (substrate thickness, *D*).

$$Q = mc\left(\frac{dT}{dt}\right)_{heating} + hA_1(T - T_0) + \frac{\lambda A_2(T-T_0)}{\delta} \quad (2)$$

Simulation

This simulation is carried out to simulate the different temperature profiles of individual locations within the substrate and surrounding the melt. These temperature profiles can be combined to generate thermal gradient graphs that allow the evaluation of the HAZs by identifying the corresponding austenitising temperature range for the material M2 HSS used for this study. Two initial substrate temperatures, T_0 = 25°C (room temperature) and T_0 =180°C (preheating), were involved. The final temperature *T* was set at its solidus temperature, 1502K obtained from the M2

HSS phase diagram (Roberts et al. 1998) at which the material starts the phase change to liquid. By evaluating the resultant cross sections of different melts produced by their respective laser scan speed and substrate temperature, the convective and convection area (A_1 and A_2 respectively) can be obtained and effective power Q can be calculated from equation (2).

The peak temperatures at different locations (x, y, z) in μm away from the moving origin (where y is the centre axis and has the value *0*) in order to plot the thermal gradient have z values set at 30, 40, 50, 60, 70 & 80. The value of x was not defined as it is dependent on the scan speed and time involved. The peak temperatures at the same location were simulated to be different at different integration limits, t = 0.005s, 0.01s and 0.015s. At integration limits, t = 0.02, 0.05, 0.5 and 1, the peak temperatures of the same location were simulated to be the same. This suggested that simulations should be carried out at integration limits, t > 0.02s for steady state conditions to take place. Hence, integration limit, t = 0.05 was used to simulate the peak temperatures in this work. Figure 2a shows an example of a simulated thermal graph which has a peak temperature of 1488K at location (17400, 0, 50) at t = 0.05s with scan speed 350 mm/s and substrate temperature of 180°C

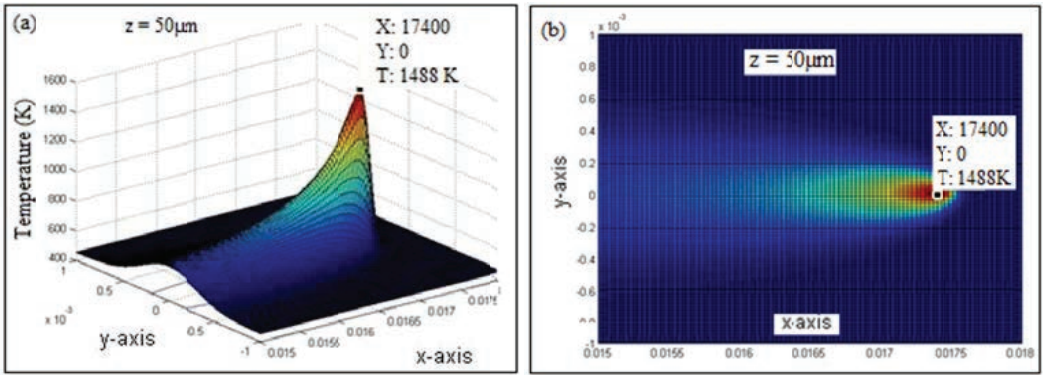

Figure 2. Thermal graph at a fixed z depth, 50μm (a) Isometric view, (b) Top view.

RESULTS AND DISCUSSION

Thermal gradient

Thermal gradient is a physical quantity used to describe the nature of temperature change around a particular location. In this simulation work, the thermal graphs at different z depths along the centre y-axis were generated at different scan speeds (250 mm/s and 350 mm/s) and substrate temperatures (25°C and 180°C). The peak temperature values were recorded and plotted against the z-axis to generate the thermal gradient. Subsequently, the austenitic temperature range and its corresponding range of HAZ were identified as seen in Figure 3.

The range of simulated HAZs with the proposed model in this work was validated experimentally. Scan track experiments were carried out with scan speeds 250 mm/s and 350 mm/s under two different substrate temperatures, 25°C and 180°C. Table 1 shows the overall experimental results compared against the simulated results.

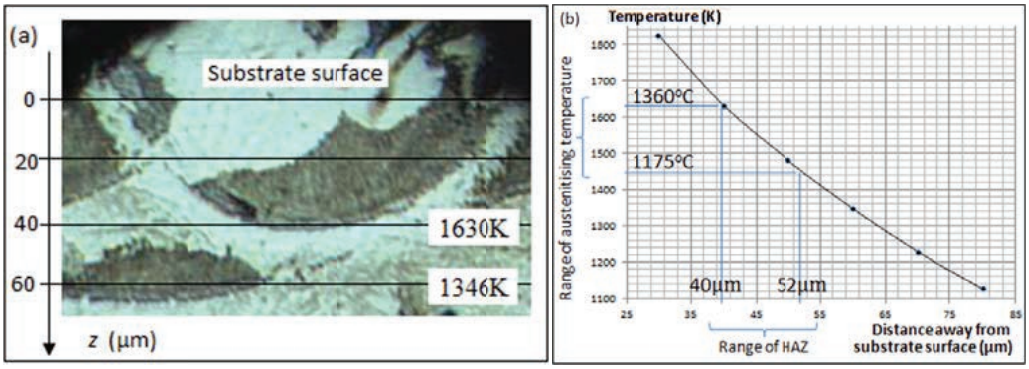

Figure 3. (a) Peak temperatures at different depths away from the substrate surface, (b) Graphical thermal gradient representation with HAZ range identified.

Table 1. Summary of simulated and experimented HAZ results

Laser Scan Speed (mm/s)	Range of Heat Affected Zone (μm)	
	Experimental	Simulated
250 (25°C)	42 - 55	48 - 58
250 (180°C)	43 – 56	45 – 56.5
350 (25°C)	37 - 49	38 – 46.5
350 (180°C)	42 – 51.5	40 - 52

Cooling rate

The cooling rate within the HAZ was simulated in this work by setting different two integrating limits at t = 0.05s and 0.06s involved during the SLM process. The cooling rate was calculated from simulated thermal graphs at a location (x, y, z) in μm where the density heat source has moved along the x-axis (x = 17400 at t = 0.05s), y is the centre axis which has a value 0, and z is the middle of the HAZ which has a fixed value of 48.15 μm. Using the same example from Figure 3, the peak temperature of 1539K was recorded at the location (17400, 0, 46.75) from the generated graph at t = 0.05s as shown in Figure 5(a). Another graph was then generated with t = 0.06s and a temperature of 582.3K was obtained at the same location, (17400, 0, 46.75) shown in Figure 5(b). Hence, the theoretical cooling rate is calculated to be 95,670 K/s over a time of 0.01s.

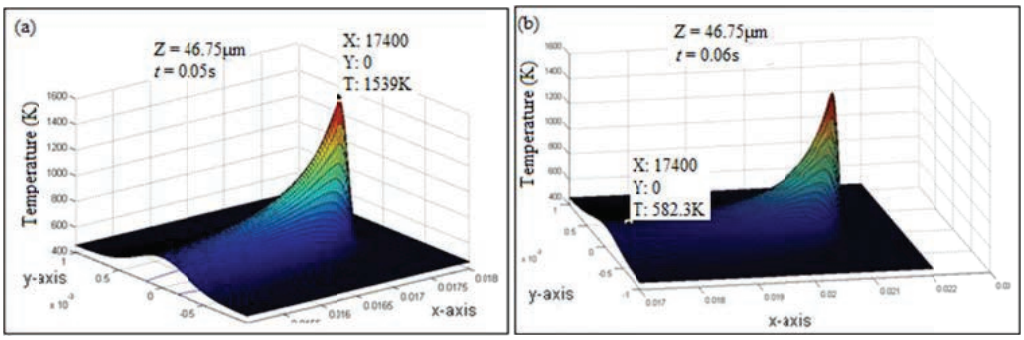

Figure 5. Temperature of location (17400, 0, 46.75) at (a) t =0.05s and (b) t =0.05s.

Discussion

While the cooling rate simulated in this work could not be validated in the SLM process due to absence of appropriate monitoring equipment at such a scale, literature studies revealed that cooling rates of similar laser melting processes and simulations (Safdar et al. 2006, Duff et al. 2007, Safdar et al. 2007) ranged from 10^4 to 10^6 K/s (Guan et al. 2010) to as high as 10^{12} K/s (Elliott et al. 1972) in laser related melting process such as welding, melting and quenching. These indicated that the simulated cooling rates in this work were reasonable. In addition, the simulated cooling rates were higher than the cooling rate of 10^3 K/s during quenching process (Hasan et al. 2011) in the conventional hardening heat treatment which would result in retained austenite.

The ranges of HAZs obtained from the generated thermal gradients for each process condition were very close to the experimental results although they were not exactly identical. Some inherent errors were present due to the difficulty in identifying the exact experimental starting and ending points of the HAZ. It was observed that the start of the HAZ begins distinctively from the melt boundary while the HAZ ended gradually into the substrate. Nevertheless, the resultant microstructure consisted of a phase evolution between alternating ferrite and austenite formed during the SLM process (Liu et al. 2011, Liu et al. 2013).

REFERENCES

[1] Elliott, W. A., Gagliano, F. P. and Krauss, G. (1972). "Rapid Cooling by Laser Melt Quenching." Applied Physics Letters **21**(1): 23-25.

[2] Roberts, G. A., Krauss, G., Kennedy, R. and Kennedy, R. L. (1998). Tool Steels, ASM International.

[3] Lancaster, J. F. (1999). Metallurgy of Welding. Abington, Abington Publishing.

[4] Shao, T. M., Lin, X. C. and Zhou, M. (2001). "Absorption of some powder materials to YAG laser." Science in China Series a-Mathematics Physics Astronomy **44**: 489-494.

[5] Kou, S. (2003). Welding Metallurgy. New jersy, John Wiley & Sons Inc.

[6] Nguyen, N. T. (2004). Thermal Analysis of Welds. Australia, WIT Press.

[7] Goldak, J. A. and Akhlaghi, M. (2005). Computational Welding Mechanics. Boston, Springer Science+Business Media Inc.

[8] Grum, J. and Slabe, J. M. (2006). "Effect of laser-remelting of surface cracks on microstructure and residual stresses in 12Ni maraging steel." Applied Surface Science **252**(13): 4486-4492.

[9] Safdar, S., Lin, L. and Sheikh, M. A. (2006). "Numerical Analysis of the Effects of non-Conventional Laser Beam Geometries During Laser Melting of Metallic Materials." Journal of Physics D-Applied Physics **40**.

[10] Duff, W. H. and Zhigilei, L. V. (2007). Computational Study of Cooling rates and Recrystallisation Kinetics in Short Pulse Laser Quenching of Metal Targets. 8th International Conference on Laser Ablation. Banff, Canada, IOP Publishing**:** 413 - 417.

[11] Safdar, S., Li, L. and Sheikh, M. A. (2007). "Numerical analysis of the effects of non-conventional laser beam geometries during laser melting of metallic materials." Journal of Physics D-Applied Physics **40**(2): 593-603.

[12] Guan, Y. C., Zhou, W., Li, Z. L. and Zheng, H. Y. (2010). Study on the Solidification Microstructure in AZ91D Mg Alloy After Laser Surface Melting. Singapore, Singapore Institute of Manufacturing Technology and Nanyang Technological University.

[13] Averyanova, M., Bertrand, P. and Verquin, B. (2011). "Studying the influence of initial powder characteristics on the properties of final parts manufactured by the selective laser melting technology." Virtual and Physical Prototyping **6**(4): 215-223.

[14] Hasan, H., Peet, M., Jalil, J. and Bhadeshia, H. (2011). "Heat transfer coefficients during quenching of steels." Heat & Mass Transfer **47**(3): 315-321.

[15] Liu, Z. H., Chua, C. K., Leong, K. F., Kempen, K., Thijs, L., Yasa, E., Humbeeck, J. V. and Kruth, J. P. (2011). A Preliminary Investigation on Selective Laser Melting of M2 High Speed Steel. 5th International Conference on Advanced Research and Rapid Prototyping. Leiria, Portugal. 28 Sep to 01 Oct 2011, CRC Press**:** 339 - 346.

[16] Liu, Z. H., Zhang, D. Q., Chua, C. K. and Leong, K. F. (2013). "Crystal structure analysis of M2 high speed steel parts produced by selective laser melting." Materials Characterization **84**(0): 72-80.

[17] Liu, Z. H., Zhang, D. Q., Leong, K. F. and Chua, C. K. (2013). Melt Characterisation of M2 High Speed Steel in Selective Laser Melting. Advanced Research in Virtual and Rapid Prototyping, Leiria, Portugal, CRC Press.

[18] Zhang, D. Q., Liu, Z. H. and Chua, C. K. (2013). Investigation of Forming Process of Copper Alloys via Selective Laser Melting. Advanced Research in Virtual and Rapid Prototyping, Leiria, Portugal, CRC Press.

[19] Loh, L. E., Liu, Z. H., Zhang, D. Q., Mapar, M., Sing, S. L., Chua, C. K. and Yeong, W. Y. (2014). "Selective Laser Melting of aluminium alloy using a uniform beam profile." Virtual and Physical Prototyping **9**(1): 11-16.

[20] Chua, C. K., Leong, K. F. and Lim, C. S. (2010). Rapid Prototyping - Principles and Applications. Singapore, World Scientific Publishing Co. Pte. Ltd.

[21]